PTEP

Prog. Theor. Exp. Phys. **2023** 033B04(24 pages)
DOI: 10.1093/ptep/ptad021

IYBSSD2022
International Year
of Basic Sciences
for Sustainable Development

A model of pseudo-Nambu–Goldstone dark matter from a softly broken $SU(2)$ global symmetry with a $U(1)$ gauge symmetry

Tomohiro Abe[1,*] and Yu Hamada[2]

[1] *Department of Physics, Faculty of Science and Technology, Tokyo University of Science, Noda, Chiba 278-8510, Japan*
[2] *Theory Center, High Energy Accelerator Research Organization (KEK), Tsukuba 305-0801, Japan*
*E-mail: abe.tomohiro@rs.tus.ac.jp

Received December 19, 2022; Revised February 1, 2023; Accepted February 6, 2023; Published February 7, 2023

A model of the pseudo-Nambu–Goldstone (pNG) dark matter (DM) is proposed. We assume that there is an $SU(2)_g$ global symmetry and a $U(1)_X$ gauge symmetry in the dark sector, and they are spontaneously broken into a $U(1)_D$ global symmetry after a scalar field develops a vacuum expectation value. We add a soft symmetry-breaking term that breaks the $SU(2)_g$ global symmetry into the $U(1)_g$ global symmetry explicitly. Our model predicts a stable complex pNG particle under the $U(1)_D$ global symmetry. One of the virtues of the pNG DM models is that the models can explain the current null results of the direct detection experiments. The small momentum transfer suppresses the scattering amplitudes thanks to the low-energy behavior of the Nambu–Goldstone boson. In our model, the soft symmetry-breaking term is uniquely determined. This is the advantage of our model compared to some earlier works in which some soft symmetry-breaking terms cannot be forbidden but are simply assumed to be absent to avoid the constraints from the direct detection experiments. We calculate the thermal relic abundance of the pNG DM and find that the model can explain the measured value of the DM energy density under some constraints from perturbative unitarity.

Subject Index B40, B71

1. Introduction

A popular scenario about dark matter (DM) production is that DM particles interact with standard model (SM) particles and were in the thermal bath made by the SM particles in the early universe. The interaction rate is reduced as the universe expands, and the interactions between the DM and SM particles are eventually decoupled. After the decoupling, the DM number density per comoving volume is fixed. In this scenario, the DM in the current universe is the thermal relic, and the measured value of the DM energy density [1] requires some small but non-zero DM annihilation cross section into the SM particles. The canonical value is $\langle \sigma v \rangle \simeq 10^{-26}\ \mathrm{cm}^3\,\mathrm{s}^{-1}$. The crossing symmetry of the Feynman diagrams implies that DM–SM elastic scatterings can also happen. The DM direct detection experiments have been trying to detect

Funded by SCOAP[3]. SCOAP3 and OUP support the goals of the International Year of Basic Sciences for Sustainable Development

such scattering processes over the decades. However, there are no clear signals of the DM–SM scatterings, and the experiments give stringent upper bounds on the DM–nucleon scattering cross section [2–4]. It is necessary to suppress the DM–SM scattering process while keeping the DM annihilation cross section if the DM particles are the thermal relic.

Pseudo-Nambu–Goldstone (pNG) DM models can explain the null results of the direct detection experiments while keeping the canonical value of the DM annihilation cross section into the SM particles [5]. In the pNG DM models, the DM–SM scattering amplitude is proportional to t, where t is the Mandelstam variable and is the momentum transfer squared at low energy. Since the momentum transfer in the direct detection experiments is typically small, the scattering amplitude is highly suppressed.[1] As a result, the models can explain the null results of the direct detection experiments.

In the model proposed in Ref. [5], a Nambu–Goldstone (NG) boson is accompanied by spontaneous symmetry breaking of a $U(1)$ global symmetry after a complex scalar field S develops a vacuum expectation value (VEV). The global symmetry is also broken explicitly by the soft symmetry-breaking term $S^2 + S^{*2}$, and thus the NG boson becomes massive. Other soft symmetry-breaking terms are also possible but are assumed to be absent because they give unsuppressed contributions to the scattering amplitudes. This assumption is reasonable to explain the experimental results, but it is more satisfactory if we can forbid those terms by some symmetries. Moreover, the soft symmetry-breaking term explicitly breaks the global $U(1)$ symmetry into a global Z_2 symmetry, and this Z_2 symmetry is spontaneously broken. Hence the model [5] suffers from the domain-wall problem [7].

A possible mechanism to have (almost) only the quadratic term and to avoid the domain-wall problem has already been discussed in Ref. [5]. Models that explain why only the $S^2 + S^{*2}$ term arises are proposed in Refs. [8–11]. Those models utilize the $U(1)_{B-L}$ gauge symmetry to restrict the soft symmetry-breaking terms. The $U(1)_{B-L}$ gauge symmetry is spontaneously broken at high energy, and the pNG model proposed in Ref. [5] arises as the low-energy effective theory.[2] The models predict that the DM is not absolutely stable and decays eventually. To make the DM long-lived particle, the scale of the $U(1)_{B-L}$ breaking is assumed to be very high around the GUT scale. In Ref. [15], the effect of the mass-dimension-one soft-breaking term $S + S^*$ is discussed. In that case, the Z_2 symmetry is also explicitly broken, and thus the domain-wall problem is absent. However, the degeneracy in the mass spectra of the scalar particles is necessary to suppress the DM–quark scattering amplitude. Analyses with other explicit breaking terms are discussed in Refs. [16,17].

In this paper, we construct a model that allows only the mass-dimension-two soft symmetry-breaking terms by a gauge symmetry. The gauge symmetry is broken around the electroweak or TeV scale in contrast to the pNG models with the $U(1)_{B-L}$ gauge symmetry. In our model, any discrete symmetry is not spontaneously broken and the domain-wall problem is absent.

[1] However, this is not the case if the mediator mass is not larger than the momentum transfer [6].

[2] Note that, in general, the domain-wall problem can be avoided if the soft-breaking term arises from a VEV that spontaneously breaks a continuous (simple) symmetry G into the Z_2 symmetry, in which it is not necessary to gauge G. In fact, suppose that two scalar VEVs trigger a two-step symmetry breaking $G \to Z_2 \to 1$, in which the pNG model in Ref. [5] arises after the first symmetry breaking. Since $\pi_0(G) = 0$ and $\pi_1(G/Z_2) = Z_2$, cosmic strings with the topological charge Z_2 appear at the first phase transition and become connected by domain walls at the second one. Regardless of whether G is global or local, the domain walls shrink well before they dominate the energy density of the universe; see Sect. 13.6 in Ref. [12] and also Refs. [13,14].

The rest of this paper is organized as follows. In Sect. 2, we introduce our model setup. In Sect. 3, we show that the DM–SM elastic scattering amplitude is suppressed at the tree level. Some constraints from the perturbative unitarity, Higgs invisible decay, and cosmic strings are discussed in Sect. 4. We show that the model can explain the measured value of the DM energy density in Sect. 5. In Sect. 6, we consider the direct detection of the pNG DM at the loop level. In Sect. 7, we also consider a two-component DM scenario in our model. Section 8 is devoted to the conclusion. We present cosmic string solutions in our model in Appendix A. The calculated results of the scattering amplitudes in the direct detection at the loop level are provided in Appendix B.

2. Model

We introduce a complex scalar field ϕ that transforms under an $SU(2)_g$ global symmetry and a $U(1)_X$ gauge symmetry as[3]

$$\phi \to e^{iT^a\theta_g^a} e^{i\frac{1}{2}\theta_X(x)}\phi, \tag{1}$$

where T^a is the $SU(2)_g$ generator. Under the symmetry of the SM sector, ϕ is a singlet. All the SM particles are singlets under the $SU(2)_g \times U(1)_X$ symmetry. We assume that ϕ develops a VEV,

$$\langle\phi\rangle = \begin{pmatrix} 0 \\ \frac{v_s}{\sqrt{2}} \end{pmatrix}, \tag{2}$$

and breaks the symmetry spontaneously as $SU(2)_g \times U(1)_X \to U(1)_D$, where $U(1)_D$ is a global symmetry and is expressed as

$$\phi \to e^{iT^3\theta_D} e^{i\frac{1}{2}\theta_D}\phi = \begin{pmatrix} e^{i\theta_D} & 0 \\ 0 & 1 \end{pmatrix}\phi. \tag{3}$$

This spontaneous symmetry breaking generates three NG bosons. One is the would-be NG boson that is eaten by the $U(1)_X$ gauge boson. The other two are massless NG bosons.

To make the two NG bosons massive, we introduce an explicit symmetry-breaking term that softly breaks $SU(2)_g$ into $U(1)_g$,

$$\phi^\dagger T^3 \phi. \tag{4}$$

This soft-breaking term[4] changes the symmetry-breaking pattern. After ϕ develops the VEV, $U(1)_g \times U(1)_X$ is spontaneously broken into $U(1)_D$, and we obtain a would-be NG boson and two pNG bosons. The $U(1)_D$ global symmetry makes the pNG bosons stable, and thus these two pNG bosons are DM candidates. Thanks to the $U(1)_X$ gauge symmetry, we cannot write down other soft symmetry-breaking terms that explicitly break the global $SU(2)_g$ symmetry. Therefore, we can explain why the soft symmetry-breaking term is the mass-dimension-two in our setup.

We also impose that the new sector is symmetric under the charge conjugation,

$$\phi \to \phi^*, \tag{5}$$

[3] A model utilizing an $SU(2)$ global symmetry without any gauge symmetries is discussed in Ref. [18].

[4] We can consider $\sum_a c^a \phi^\dagger T^a \phi$, which looks like more general soft-breaking terms. However, after the field redefinition, $\phi \to e^{iT^a\theta^a}\phi$, these terms transform as $\sum_a c^a \phi^\dagger T^a \phi \to \sum_{a,b} O^{ba} c^a \phi^\dagger T^b \phi$, where $O^{ba} = \left(e^{-iX^c\theta^c}\right)_{ba}$, and $(X^c)_{ab} = -i\epsilon^{cab}$. Since O is a three-by-three orthogonal matrix, the norms of $\vec{c}$ and $O\vec{c}$ are the same. Thus we can make $O\vec{c} = (0, 0, |\vec{c}|)$ by choosing $\vec{\theta}$ appropriately. Therefore, we can take $c^a = c\delta^{a3}$ without loss of generality and obtain Eq. (4).

$$V_\mu \to -V_\mu, \tag{6}$$

where V_μ is the $U(1)_X$ gauge boson. All the SM particles are singlets under this charge conjugation. This symmetry is Z_2 but not broken by the VEV of ϕ. This symmetry also forbids the gauge kinetic mixing between the $U(1)_X$ and $U(1)_Y$ gauge fields.[5]

Now we have two DM candidates. One is the pNG DM that is stabilized by the $U(1)_D$ global symmetry and the Z_2 symmetry. The other is the gauge boson V_μ that can be stabilized by the Z_2 symmetry. The model contains a multi-component DM scenario depending on the mass spectra. If the mass of V is larger than twice the mass of the pNG DM, namely $m_V > 2m_\chi$, then V can decay into $\chi\chi^\dagger$ and thus only the pNG bosons are DM candidates. On the other hand, if $m_V < 2m_\chi$, then V cannot decay due to the Z_2 symmetry and χ cannot decay due to the $U(1)_D$ symmetry, and thus the model has two DM components.

2.1. *Lagrangian*

Under the setup, the renormalizable Lagrangian is given by

$$\mathcal{L} = \mathcal{L}|_{\text{SM w/o Higgs potential}} + D^\mu\phi^\dagger D_\mu\phi - \frac{1}{4}V^{\mu\nu}V_{\mu\nu} - V_{\text{SU(2)-global}} - V_{\text{soft}}, \tag{7}$$

where

$$D_\mu\phi = \partial_\mu\phi + i\frac{1}{2}g_D V_\mu\phi, \tag{8}$$

$$V_{\mu\nu} = \partial_\mu V_\nu - \partial_\nu V_\mu, \tag{9}$$

$$\begin{aligned} V_{\text{SU(2)-global}} = &+\mu_H^2 H^\dagger H + \mu_\phi^2\phi^\dagger\phi \\ &+ \lambda_H\left(H^\dagger H\right)^2 + \lambda_\phi\left(\phi^\dagger\phi\right)^2 + \lambda_{H\phi}(H^\dagger H)\left(\phi^\dagger\phi\right), \end{aligned} \tag{10}$$

$$V_{\text{soft}} = \mu_\chi^2\left(\phi^\dagger T^3\phi\right), \tag{11}$$

and H is the SM Higgs field. As we have already discussed, the soft-breaking term, V_{soft}, contains only a mass-dimension-two operator. Mass-dimension-one operators and mass-dimension-three operators are forbidden by the $U(1)_X$ gauge symmetry.

We make a brief comment on mass-dimension-four operators that explicitly break the $SU(2)_g$ global symmetry. In our setup, we neglect those terms to explain the current null results of the dark matter direct detection experiments. Suppose that the global $SU(2)_g$ is exact. Then, the NG boson scattering amplitude is suppressed by the small momentum at low energy. This is also true if the global $SU(2)_g$ is broken by the mass-dimension-two operator because it does not modify the structure of the interaction. We utilize this nature in our model to suppress the DM–quark scattering amplitude, which we will show in Sect. 3. If we add the mass-dimension-four global $SU(2)_g$-breaking terms, the structure of the interactions is modified, and the scattering amplitude is not suppressed at low energy in general as discussed in Ref. [5].

[5] If we do not impose the Z_2 symmetry and introduce the gauge kinetic mixing, then the amplitude of the pNG DM scattering of the SM particle is unsuppressed by the small momentum transfer [19].

2.2. *Scalar masses and couplings*

Component fields and VEVs are parametrized as

$$H = \begin{pmatrix} i\pi_{W^+} \\ \frac{v+\sigma-i\pi_Z}{\sqrt{2}} \end{pmatrix}, \ \phi = \begin{pmatrix} i\chi \\ \frac{1}{\sqrt{2}}(v_s + s - i\chi_V) \end{pmatrix}, \tag{12}$$

where v and v_s are the VEVs and π_{W^+}, π_Z, and χ_V are the would-be NG bosons for W^+, Z, and V, respectively. The stationary condition of this vacuum imposes the following relations for the mass parameters:

$$\mu_H^2 = -v^2\lambda_H - \frac{1}{2}v_s^2\lambda_{H\phi}, \tag{13}$$

$$\mu_\phi^2 = \frac{\mu_\chi^2}{2} - \frac{1}{2}v^2\lambda_{H\phi} - v_s^2\lambda_\phi. \tag{14}$$

The mass terms of the physical scalar particles are given by

$$\mathcal{L}_{\text{mass}}^{\text{scalar}} = -\mu_\chi^2\chi^\dagger\chi - \frac{1}{2}\begin{pmatrix}\sigma & s\end{pmatrix}\begin{pmatrix} 2\lambda_H v^2 & \lambda_{H\phi}vv_s \\ \lambda_{H\phi}vv_s & 2\lambda_\phi v_s^2 \end{pmatrix}\begin{pmatrix}\sigma \\ s\end{pmatrix}. \tag{15}$$

It is found that the mass of the DM m_χ is given by μ_χ, namely $m_\chi^2 = \mu_\chi^2$. The mass eigenstates that are denoted by h and h' are obtained by diagonalizing the two-by-two mass matrix above. The relation between the mass eigenstates and component fields is given by

$$\begin{pmatrix}\sigma \\ s\end{pmatrix} = \begin{pmatrix} c_\theta & s_\theta \\ -s_\theta & c_\theta \end{pmatrix}\begin{pmatrix} h \\ h' \end{pmatrix}, \tag{16}$$

where $c_\theta = \cos\theta_h$ and $s_\theta = \sin\theta_h$. The mass eigenvalues and the mass matrix are related by the mixing angle as follows:

$$\begin{pmatrix} 2\lambda_H v^2 & \lambda_{H\phi}vv_s \\ \lambda_{H\phi}vv_s & 2\lambda_\phi v_s^2 \end{pmatrix} = \begin{pmatrix} c_\theta & s_\theta \\ -s_\theta & c_\theta \end{pmatrix}\begin{pmatrix} m_h^2 & 0 \\ 0 & m_{h'}^2 \end{pmatrix}\begin{pmatrix} c_\theta & -s_\theta \\ s_\theta & c_\theta \end{pmatrix}, \tag{17}$$

where m_h and $m_{h'}$ are the masses of h and h', respectively. The quartic couplings are expressed by m_h, $m_{h'}$, and θ_h as

$$\lambda_H = \frac{m_h^2c_\theta^2 + m_{h'}^2s_\theta^2}{2v^2}, \tag{18}$$

$$\lambda_\phi = \frac{m_h^2s_\theta^2 + m_{h'}^2c_\theta^2}{2v_s^2}, \tag{19}$$

$$\lambda_{H\phi} = \frac{\left(m_{h'}^2 - m_h^2\right)s_\theta c_\theta}{vv_s}. \tag{20}$$

The χ–SM fermion elastic scattering processes are mediated by exchanging h and h'. The relevant couplings for the processes are given by

$$\mathcal{L} \supset -g_{\chi\chi h}\chi^\dagger\chi h - g_{\chi\chi h'}\chi^\dagger\chi h' - g_{\bar{f}fh}\bar{f}fh - g_{\bar{f}fh'}\bar{f}fh', \tag{21}$$

where

$$g_{\chi\chi h} = -\frac{m_h^2}{v_s}s_\theta, \tag{22}$$

$$g_{\chi\chi h'} = +\frac{m_{h'}^2}{v_s}c_\theta, \tag{23}$$

$$g_{\bar{f}fh} = +\frac{m_f}{v}c_\theta, \tag{24}$$

$$g_{\bar{f}fh'} = +\frac{m_f}{v}s_\theta. \tag{25}$$

Here f stands for the SM fermions.

2.3. *Gauge boson mass and interaction terms*

After ϕ develops the VEV, the $U(1)_X$ gauge boson acquires mass,

$$\mathcal{L} \supset \frac{m_V^2}{2}V^\mu V_\mu, \tag{26}$$

where

$$m_V^2 = \frac{1}{4}g_D^2 v_s^2. \tag{27}$$

The relevant interaction terms containing V for the following analysis are given by

$$\mathcal{L} \supset -ig_{V\chi\chi}V^\mu\left(\chi^\dagger \overleftrightarrow{\partial}_\mu \chi\right) + \frac{1}{2}g_{VVh}V^\mu V_\mu h + \frac{1}{2}g_{VVh'}V^\mu V_\mu h', \tag{28}$$

where

$$g_{V\chi\chi} = \frac{m_V}{v_s}, \tag{29}$$

$$g_{VVh} = -\frac{2m_V^2}{v_s}s_\theta, \tag{30}$$

$$g_{VVh'} = \frac{2m_V^2}{v_s}c_\theta. \tag{31}$$

2.4. *Parameters*

There are seven model parameters in the scalar and the new gauge sectors:

$$\left(\mu_H^2,\ \mu_s^2,\ \lambda_H,\ \lambda_\Phi,\ \lambda_{H\Phi},\ \mu_\chi^2,\ g_D\right). \tag{32}$$

Instead of using these parameters, we choose the following seven parameters as inputs in the following analysis:

$$\left(v,\ v_s,\ m_h,\ m_{h'},\ \theta_h,\ m_\chi,\ m_V\right). \tag{33}$$

Among these parameters, v and m_h are already known, $v \simeq 246$ GeV and $m_h \simeq 125$ GeV [20], and thus we have five free parameters $\left(v_s,\ m_{h'},\ \theta_h,\ m_\chi,\ m_V\right)$.

3. Tree-level DM–quark scattering amplitudes

DM scattering off the quark is the essential process for DM direct detection experiments. This χq scattering process is mediated by h and h' exchanging diagrams in the t-channel. Its amplitude is given by

$$\begin{aligned} i\mathcal{M} &= -ig_{\chi\chi h}\frac{i}{t-m_h^2}(-ig_{\bar{f}fh})\bar{u}u - ig_{\chi\chi h'}\frac{i}{t-m_{h'}^2}(-ig_{\bar{f}fh'})\bar{u}u \\ &= -i\frac{m_f}{vv_s}s_\theta c_\theta\left(-\frac{m_h^2}{t-m_h^2}+\frac{m_{h'}^2}{t-m_{h'}^2}\right)\bar{u}u \\ &= -i\frac{m_f}{vv_s}s_\theta c_\theta\left(-\frac{t}{t-m_h^2}+\frac{t}{t-m_{h'}^2}\right)\bar{u}u. \end{aligned} \tag{34}$$

Since $|t| \ll m_h^2, m_{h'}^2$ in the direct detection experiments, this amplitude is suppressed by $\frac{t}{m_h^2}$ and $\frac{t}{m_{h'}^2}$. As a result, the model predicts a very small spin-independent cross section in the direct detection experiments. This is the virtue of the pNG DM models.

At the loop level, however, the scattering amplitude that is not suppressed by the small momentum transfer can be induced [21–23]. We discuss the loop effect in Sect. 6.

For $m_V < 2m_\chi$, both χ and V are stable. Then V is also a DM component, and we have to consider the Vq scattering process. The scattering amplitude is given by

$$\begin{aligned} i\mathcal{M} &= ig_{VVh}\frac{i}{t-m_h^2}(-ig_{\bar{f}fh})\bar{u}u + ig_{VVh'}\frac{i}{t-m_{h'}^2}(-ig_{\bar{f}fh'})\bar{u}u \\ &= i\frac{2m_f}{vv_s}s_\theta c_\theta\left(-\frac{m_V^2}{t-m_h^2}+\frac{m_V^2}{t-m_{h'}^2}\right)\bar{u}u. \end{aligned} \tag{35}$$

In contract to χq scattering, the Vq scattering amplitude is not suppressed. Therefore, the results from the DM direct detection experiments give constraints on the mass and the number density of V.

The purpose of the current paper is to investigate whether the model given in Eq. (7) is a viable pNG DM model. Thus we mainly focus on the single-component DM scenario where $m_V > 2m_\chi$. The multi-component scenario where $m_V < 2m_\chi$ is briefly discussed in Sect. 7.

4. Constraints

In this section, we discuss constraints from the perturbative unitarity, the Higgs invisible decay, and cosmic strings.

4.1. *Perturbative unitarity*

We find the constraints on the scalar and gauge couplings from the perturbative unitarity (PU) bound [24]. Two-to-two scattering amplitudes at high energy can be decomposed into partial waves,

$$\mathcal{M} = 16\pi\sum_\ell (2\ell+1)P_\ell(\cos\theta)a_\ell, \tag{36}$$

where P_ℓ is the Legendre polynomial, and $\cos\theta$ is the scattering angle. In general, there are inelastic scatterings, and thus a_ℓ is a matrix. Unitarity requires each eigenvalue of a_ℓ to satisfy

$$|\mathrm{Re}\, a_\ell| \le \frac{1}{2}. \tag{37}$$

We utilize this inequality to find the constraints on the scalar and gauge couplings.

4.1.1. *Scalar quartic couplings.*

Two-to-two scattering processes containing only the scalar bosons give the following PU bound on the scalar quartic couplings:

$$|\lambda_H| < 4\pi, \tag{38}$$

$$|\lambda_{H\phi}| < 8\pi, \tag{39}$$

$$|\lambda_\phi| < 4\pi, \tag{40}$$

$$\left|3\lambda_H + 3\lambda_\phi \pm \sqrt{9(\lambda_\phi-\lambda_H)^2+4\lambda_{H\phi}}\right| < 8\pi. \tag{41}$$

In the following analysis, λ_ϕ is typically the largest quartic coupling among the three quartic couplings. In that case, the condition given in Eq. (41) is essential and is reduced to

$$|\lambda_\phi| < \frac{4\pi}{3}. \tag{42}$$

4.1.2. *Gauge coupling.* We study $V\chi \to V\chi$ scattering at high energy in order to find the constraint on g_D. Here V is transversely polarized. The longitudinal mode is already taken into account in the previous subsection thanks to the equivalence theorem [24–28]. We find

$$a_0^{\lambda\lambda'} = -\frac{g_D^2}{96\pi}\lambda\lambda', \tag{43}$$

$$a_1^{\lambda\lambda'} = -\frac{g_D^2}{192\pi}\lambda\lambda', \tag{44}$$

$$a_2^{\lambda\lambda'} = -\frac{g_D^2}{960\pi}\lambda\lambda', \tag{45}$$

where λ and λ' are the helicity of V in the initial and final states, respectively. The s-wave ($\ell = 0$) gives a stringent bound. Since there are two transversely polarized states, a_0 is a two-by-two matrix. Its eigenvalues are 0 and $-\frac{g_D^2}{48\pi}$, and their absolute values should be smaller than 1/2. We find

$$g_D < \sqrt{24\pi}. \tag{46}$$

4.2. *Higgs invisible decay*

If $m_\chi < m_h/2$, then the Higgs boson decays into $\chi\chi^\dagger$. The decay width is given by

$$\Gamma(h \to \chi\chi^\dagger) = \frac{1}{16\pi}\frac{g_{\chi\chi h}^2}{m_h}\sqrt{1-\frac{4m_\chi^2}{m_h^2}}\theta(m_h - 2m_\chi). \tag{47}$$

This process is Higgs invisible decay and is being sought by the ATLAS and CMS experiments. Currently, the ATLAS[29] and CMS[30] experiments have obtained an upper bound on it as

$$\mathrm{BR}_{\mathrm{inv}} < \begin{cases} 0.11 & (\mathrm{ATLAS}) \\ 0.18 & (\mathrm{CMS}) \end{cases} \tag{48}$$

at 95% CL. The prospects of various experiments are summarized in Ref. [31],

$$\mathrm{BR}_{\mathrm{inv}} < \begin{cases} 0.019 & (\mathrm{HL\text{-}LHC}) \\ 0.0026 & (\mathrm{ILC}(250)) \\ 0.00024 & (\mathrm{FCC}) \end{cases} \tag{49}$$

at 95% CL, where FCC corresponds to the combined performance of FCC-ee$_{240}$, FCC-ee$_{365}$, FCC-eh, and FCC-hh. The prospects for the ILC and FCC are obtained by combining with the HL-LHC.

4.3. *DM relic abundance from cosmic strings*

Our model admits cosmic strings (or vortex strings) [12] as non-trivial solutions of the static equations of motion. In fact, concentrating on the dark sector, the symmetry-breaking pattern $U(1)_g \times U(1)_X \to U(1)_D$ leads to the non-trivial first homotopy group of the vacuum

$$\pi_1\left(\frac{U(1)_g \times U(1)_X}{U(1)_D}\right) \simeq \pi_1\left(U(1)\right) = \mathbb{Z}\,, \tag{50}$$

which means that the solutions are characterized by the winding number $n \in \mathbb{Z}$. This model is similar to a model in Ref. [32] that admits semilocal strings [33,34] with an explicit $SU(2)$-breaking term, which is a mass-dimension-four operator like $(\phi^\dagger T^3 \phi)^2$. In our model, however, the $SU(2)_g$ symmetry is explicitly broken by the soft-breaking term, and hence the property of the string solution is different from those. We present the string solution in our model in Appendix A. In this section, we discuss their effects on cosmology, in which the detailed structure or properties of the string solution are irrelevant.

When the temperature T of the thermal bath goes below v_s, the $U(1)_g \times U(1)_X$ symmetry breaks spontaneously into $U(1)_D$, leading to the creation of cosmic strings [35,36]. The created strings form a network, whose typical length scale becomes the Hubble length $l_H(T \simeq v_s)$ within the Hubble time $t_H(T \simeq v_s)$ after creation. These strings randomly move in the expanding universe and produce closed loops by their reconnection. Thanks to the production of the loops, the number of strings per Hubble patch always remains at $\mathcal{O}(1)$, which is known as the scaling solution [12], avoiding the overclosure of the universe. Therefore, the string network itself does not affect the cosmological history.

On the other hand, the produced string loops could affect the DM relic abundance. This is because the string loops decay into light particles or gravitational waves, the former of which are nothing but the pNG DM χ. Thus the string loops give an additional contribution to the DM relic abundance besides the thermal relic one. We give a simple estimation for the former one.[6]

The time evolution of the string network can be understood analytically by the so-called velocity-dependent one-scale model [39,40]. At cosmological time t, closed loops are produced from the network with a distribution function [40]

$$f_{\rm loop}(l, t) = \frac{A}{\alpha t^4} \delta(l - \alpha t) \tag{51}$$

such that the number density of the loops produced per time with length in the range between l and $l + dl$ is given by $f_{\rm loop}(l, t)dl$. Here A and α are $\mathcal{O}(0.1)$ constants.

We consider the most "pessimistic" case, i.e., all of such loops decay by emitting only the pNG boson, which means that all the energy of the loops is converted into the DM relic abundance. For simplicity, we further assume that the closed loops decay instantaneously. Note that, before the interaction between the DM and the thermal bath is out of equilibrium, $t < t_{\rm f.o.}$, the DM supplied from the loops is washed out and its number density does not deviate from the thermal equilibrium value. Thus it is sufficient to consider only stages after the decoupling $t \geq t_{\rm f.o.}$. Then we can find that the DM number density produced from the string loops, $n_{\rm DM,\,st}$, follows the Boltzman equation

$$\frac{d}{dt} n_{\rm DM,st}(t) + 3H(t)\, n_{\rm DM,st}(t) = \int dl\, \frac{l \mu f_{\rm loop}(l,t)}{m_\chi}, \tag{52}$$

where μ is the tension of the strings $\mu \sim v_s^2$ and $H(t)$ is the Hubble parameter. Substituting Eq. (51) and introducing the yield $Y_{\rm DM,\,st} \equiv n_{\rm DM,\,st}/s$ with s the entropy density $s \sim g_* T^3$, Eq. (52) is rewritten as

$$\frac{d}{dt} Y_{\rm DM,st}(t) \simeq \frac{\mu A}{m_\chi t^3 g_* T^3}, \tag{53}$$

leading to

[6]Note that, since our string is the local one and the pNG boson is associated with the global $SU(2)_g$ symmetry, we cannot apply straightforwardly the studies on NG bosons from global $U(1)$ strings [37,38].

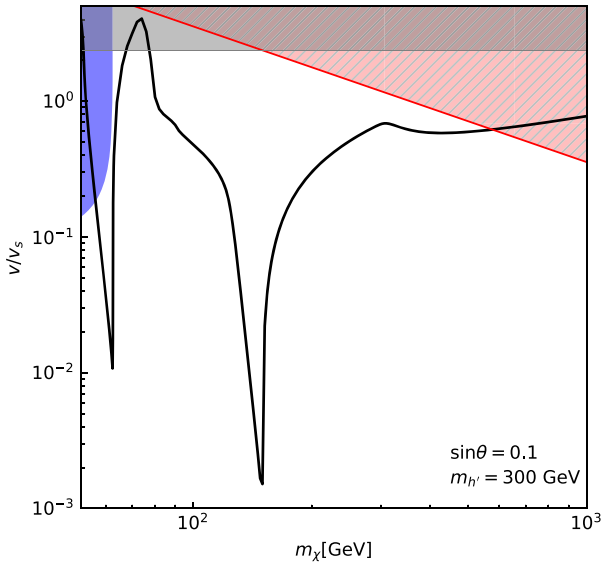

Fig. 1. The black solid curve shows the value of v_s that can explain the measured value of the dark matter energy density. In the gray shaded region, the perturbative unitarity for the scalar channel is violated. In the red hatched shaded region, the gauge coupling exceeds the value required by the perturbative unitarity. The blue shaded region around the top-left corner is excluded by the Higgs invisible decay search.

$$Y_{\mathrm{DM,st}}(\infty) \simeq \int_{t_{\mathrm{f.o.}}}^{\infty} dt\, \frac{\mu A}{m_\chi t^3 g_* T^3} \tag{54}$$

$$\sim \frac{T_{\mathrm{f.o.}}}{m_\chi} \left(\frac{v_s}{M_{\mathrm{pl}}}\right)^2, \tag{55}$$

where we have used $T^2 \sim M_{\mathrm{pl.}}/t$ and $T_{\mathrm{f.o.}}$ is the freeze-out temperature known to be given as $T_{\mathrm{f.o.}} \simeq m_\chi/25$. Therefore, compared to the correct thermal relic abundance, $Y_{\mathrm{DM}} \sim 10^{-12}$, the abundance from the loops is tiny and hence does not affect the argument presented in the next section.

5. Relic abundance

We show that the model explains the DM energy density by the thermal relic abundance of χ and $\chi^\dagger$. A $\chi\chi^\dagger$ pair annihilates into the SM particles mainly by exchanging h and h' in the s-channel. It also annihilates into hh' and $h'h'$ pairs if these processes are kinematically allowed. We calculate the relic abundance for a given parameter set and find the value of v_s that produces the right amount of DM as the thermal relic. As we mentioned at the end of Sect. 3, we focus on the parameter space where $m_V > 2m_\chi$. In the following analysis, we set $m_V = 3m_\chi$.

Figure 1 shows the value of v_s that can explain the DM energy density by the thermal relic. We use `micrOMEGAs` [41] to calculate the relic abundance. The constraints from the PU bound and the Higgs invisible decay are also shown. The PU bound for the scalar quartic couplings excludes the small v_s region. This bound is also sensitive to the choice of mixing angle θ. A smaller mixing angle requires smaller v_s to obtain the right amount of the thermal relic. Consequently, too small a mixing angle is disfavored by the PU bound for the scalar couplings. The PU bound for the gauge coupling is essential for the heavy χ regime. It gives the upper bound on m_χ. There are two dips in Fig. 1. One is at $m_\chi \simeq m_h/2$, and the other is at $m_\chi \simeq m_{h'}/2$. Pairs

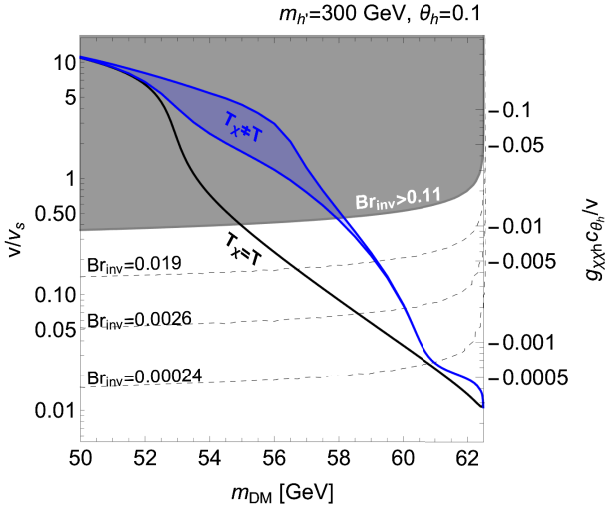

Fig. 2. The value of v_s that can explain the measured value of the dark matter energy density for a given DM mass in the Higgs funnel region. The black solid curve is obtained by the standard calculation [47]. The blue region is obtained by taking into account the early kinetic decoupling effect. The lower boundary of the blue region is determined with the assumption that all the quarks (u, d, s, c, b) contribute to the DM elastic scattering process, while the upper boundary is determined with the assumption that only the light quarks (u, d, s) contribute to the scattering process [42]. The gray shaded region is excluded by the Higgs invisible decay search by the ATLAS experiment [29]. The dashed curves show the prospects provided in Ref. [31].

of DM particles annihilate by exchanging h and h' in the s-channel and the annihilation cross section is enhanced by the h or h' resonance at those mass ranges. It is necessary to make the DM–scalar coupling smaller to obtain the right amount of DM energy density at the resonant regions. This is why we see the two dips in Fig. 1.

We focus on the Higgs funnel region where m_χ is slightly smaller than half of the SM-like Higgs boson mass. In this region, the decay of the Higgs boson into two DM particles is allowed. This Higgs invisible decay has been sought in the ATLAS and CMS experiments and will be sought in future collider experiments as well. Hence it is worth having a closer look.

In the Higgs funnel region, the DM particles in the early universe can annihilate into SM particles efficiently because of the Higgs resonance. The resonant enhancement requires a smaller coupling of the DM to the Higgs boson to obtain the right amount of the DM thermal relic. This is why we can see the sharp dip at $m_\chi \simeq m_h/2$. This small coupling makes the DM–SM elastic scattering cross section small in the early universe. As a result, kinetic decoupling may happen earlier than usual [42]. One of the authors showed that the effect of kinetic decoupling is sizable in the Higgs resonant regime in the simple pNG DM model [43]. We use the same method to estimate the value of v_s that reproduces the measured value of the DM relic abundance. For the technical details, see Ref. [43].[7]

Figure 2 shows the result in the Higgs funnel region. The black solid curve is the result obtained in the standard calculation with the assumption that kinetic equilibrium is maintained during the freeze-out. The blue curves are obtained without assuming kinetic equilibrium. As

[7] In Ref. [43], the distribution function of the DM particle is assumed to be $f(T, E) = \alpha(T_\chi)e^{-E/T_\chi}$, where T_χ is the DM temperature. This assumption would be justified if the DM self-scattering is large enough. A recent discussion on the effect of DM self-scattering is given in Ref. [44]. For the method without the introduction of the DM temperature, see Refs. [45,46].

in the original pNG DM model, we find that the effect of kinetic decoupling is significant and the coupling may be underestimated if we naively assume kinetic equilibrium in the calculation for the thermal relic. We also show the current bound and future prospects for the Higgs invisible decay search. We find that the decay branching ratio of the Higgs invisible decay can be enhanced by more than an order of magnitude.

6. Direct detection at loop level

As stated in Sect. 3, the scattering amplitude between the pNG DM χ and quarks is suppressed due to the cancellation of the h, h' exchanges at the tree level. At the loop level, on the other hand, χ has a non-zero scattering amplitude with nucleons. We here calculate the loop-level amplitude and the spin-independent (SI) cross section with nucleons, and compare the result with the current experimental bound.

The effective Lagrangian relevant to the scattering process is given as

$$\mathcal{L}_{\rm eff} = C_q^S\, m_q \chi^\dagger \chi\, \bar{q} q + C_g^S \frac{\alpha_s}{\pi} \chi^\dagger \chi\, G^a_{\mu\nu} G^{a\mu\nu}, \tag{56}$$

where C_q^S and C_g^S are Wilson coefficients. We consider only the scalar-type interaction and have ignored the twist-type one since the latter is negligible.

Then the SI cross section is given as

$$\sigma_{\rm SI} = \frac{1}{4\pi} \left(\frac{\mu_N m_N}{m_\chi} \right)^2 \left| \sum_{q=u,d,s} C_q^S f_q^N - \frac{8}{9} C_g^S f_g^N \right|^2, \tag{57}$$

where m_N and $\mu_N \equiv m_N m_\chi/(m_N + m_\chi)$ are the nucleon mass and the reduced mass, respectively. f_q^N and f_g^N are the matrix elements of the operators evaluated by the nucleon states:

$$f_q^N m_N = \langle N | \, m_q \bar{q} q \, | N \rangle \,, \tag{58}$$

$$-\frac{8}{9} f_g^N m_N = \left\langle N \frac{\alpha_s}{\pi} G^a_{\mu\nu} G^{a\mu\nu} \right\rangle N. \tag{59}$$

Their approximate values are given as [48]

$$f_u^p = 0.019, \quad f_d^p = 0.027, \quad f_u^n = 0.013, \quad f_d^n = 0.040, \quad f_s^p = f_s^n = 0.009, \tag{60}$$

$$f_g^N = 1 - f_u^N - f_d^N - f_s^N + \mathcal{O}(\alpha_s). \tag{61}$$

Now our task is to calculate the scattering amplitude with quarks and gluon at the one-loop (and QCD NLO) level taking the momentum transfer to be zero ($t \to 0$), and then to read off the Wilson coefficients from them. Note that some diagrams include the tree-level process as their sub-diagrams, and thus vanish due to the cancellation of h and h' exchanges (see Fig. 3). We evaluate the remaining diagrams in terms of the following technique. In the limit $m_\chi \to 0$ where the pNG boson becomes an exact Nambu–Goldstone boson, all diagrams cancel and the total scattering amplitude vanishes as $t \to 0$ even at the loop level [22,23]:

$$i\mathcal{M}_{\rm tot}(m_\chi) \equiv \sum_{\rm diagrams} i\mathcal{M}(m_\chi) \to 0 \quad (m_\chi \to 0). \tag{62}$$

On the other hand, the cancellation among the diagrams is not exact when $m_\chi \neq 0$. Utilizing this property, we can rewrite the amplitudes as

$$i\mathcal{M}_{\rm tot}(m_\chi) = i\mathcal{M}_{\rm tot}(m_\chi) - i\mathcal{M}_{\rm tot}(0) = \sum_{\rm diagrams} \left[i\mathcal{M}(m_\chi) - i\mathcal{M}(0) \right], \tag{63}$$

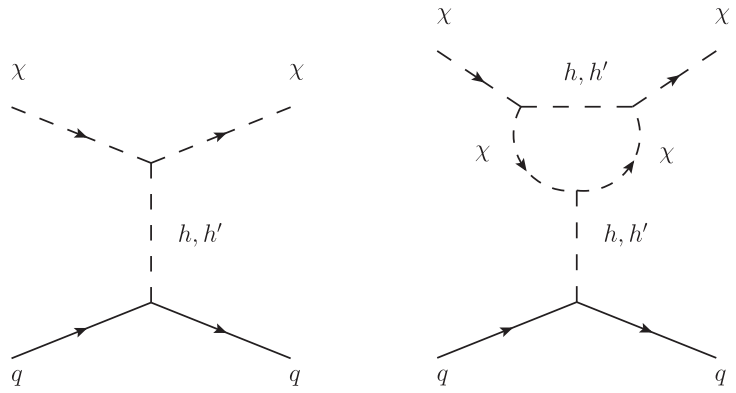

Fig. 3. Left: A tree-level scattering process between χ and quarks. Right: An example of a loop diagram that includes the tree-level one as its sub-diagram. It vanishes due to the same mechanism as the tree-level one.

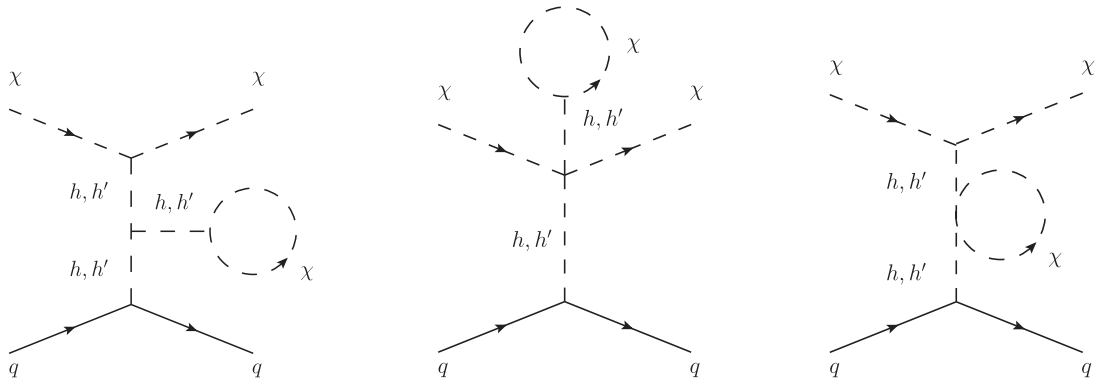

Fig. 4. An example of non-trivial cancellation. Although these three diagrams depend on m_χ explicitly, they are canceled and vanish with non-zero m_χ.

from which it follows that one does not need to calculate diagrams that are independent of m_χ since they are canceled within the bracket. In addition, tadpole diagrams that depend on m_χ are canceled by a self-energy diagram; see Fig. 4. Thus all the diagrams that we need to evaluate are the five shown in Fig. 5:

$$i\mathcal{M}_{\rm tot}(m_\chi) = \sum_{\text{diagrams in Fig. 5}} \left[i\mathcal{M}(m_\chi) - i\mathcal{M}(0) \right]. \tag{64}$$

Explicit expressions for the amplitudes and the Wilson coefficients are shown in Appendix B. We only show the numerical results of the SI cross section $\sigma_{\rm SI}$ in Fig. 6. The parameters are taken as $m_{h'} = 300\,\text{GeV}$, $m_V = 3m_\chi$, and $\sin\theta = 0.1$, and v_s is determined such that the DM relic abundance is explained by the thermal freeze-out mechanism as studied in Sect. 5. The red shaded region is excluded by the violation of the perturbative unitarity of the $U(1)_D$ gauge coupling constant, $g_D > \sqrt{24\pi}$; see Eq. (46). In the orange shaded regions, the running coupling constant $g_D(\Lambda)$ calculated by the one-loop beta function exceeds $\sqrt{24\pi}$ below $\Lambda = 100\,\text{TeV}$. The current bound by the LZ experiment [4] is shown by the blue dashed line. The gray hatched region indicates that the DM signal is hidden by the neutrino background. We find that $\sigma_{\rm SI}$ is smaller than the neutrino floor in most of the region. For the larger m_χ regime, $\sigma_{\rm SI}$ is larger than the neutrino floor and some of the region is already excluded. This is because, in that region,

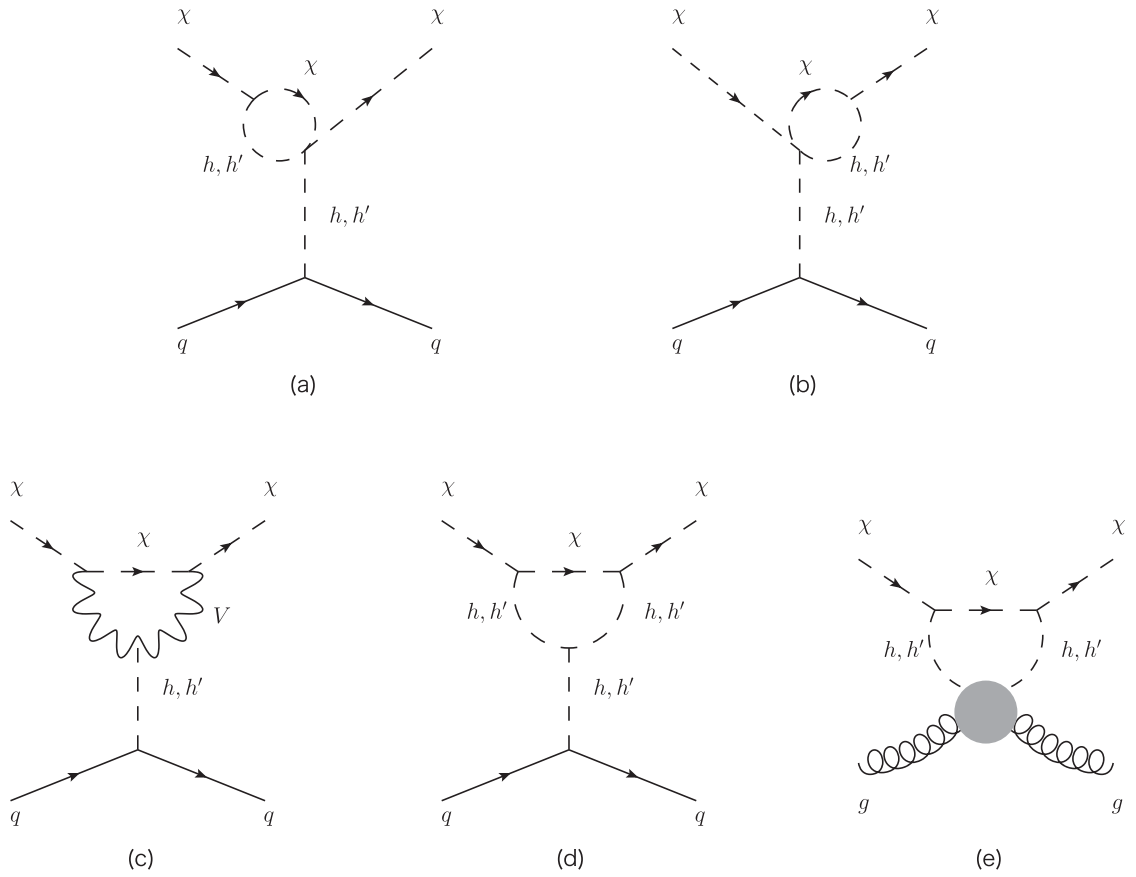

Fig. 5. Feynman diagrams relevant to the scattering with nucleons. The gray blob in the last diagram (e) indicates the QCD NLO contribution, which is dominated by the top-quark loop [21].

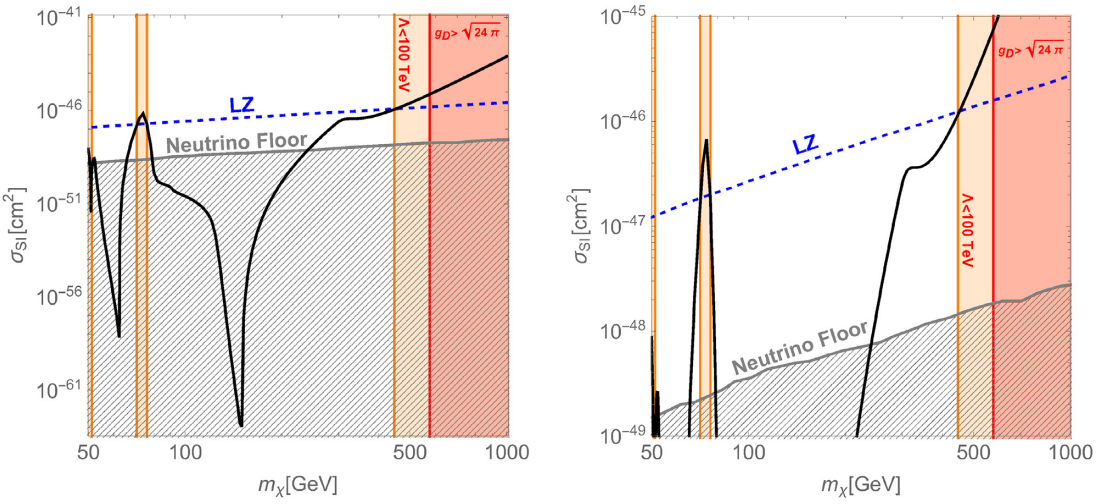

Fig. 6. Plots of the DM mass m_χ vs. the SI scattering cross section $\sigma_{\rm SI}$ between the pNG DM χ and nucleons. On the black solid line, the DM relic abundance is explained by the thermal freeze-out mechanism. The red shaded region is excluded by the perturbative unitarity of g_D. In the orange shaded regions, the running coupling constant $g_D(\Lambda)$ violates the perturbative unitarity below $\Lambda = 100$ TeV. The current upper bound by the LZ experiment is shown by the blue dashed line. The gray shaded region indicates the cosmic neutrino background. The right panel is an enlarged version of the left one.

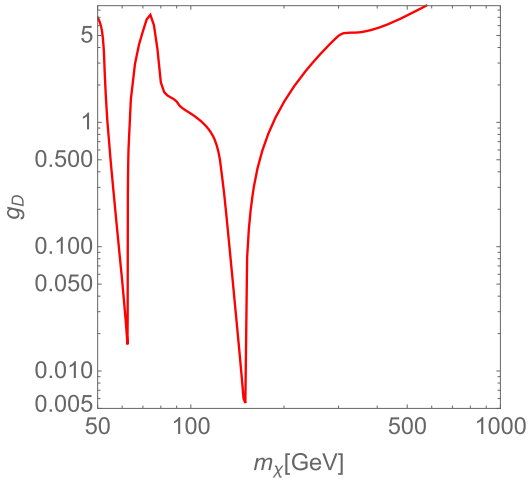

Fig. 7. The value of g_D for a given parameter set. Here we take $\sin\theta = 0.1$ and $m_V = 3m_\chi$, and v_s is given in Fig. 1.

the gauge coupling constant becomes large, as seen in Fig. 7. The diagram containing the gauge boson (Fig. 5(c)) is proportional to g_D^4, and hence gives a significantly large contribution. We conclude that, in almost all parameter space, the SI cross section $\sigma_{\rm SI}$ is far below the current experimental bound as long as we keep the value of g_D small.

7. Two-component scenario

Here we discuss the two-component scenario in this model where $m_V < 2m_\chi$. In this scenario, the DM energy density is the sum of the energy densities of χ and V, namely $\Omega h^2 = (\Omega h^2)_\chi + (\Omega h^2)_V$. We determine the value of v_s to obtain the right amount of DM energy density.

The top-left panel in Fig. 8 shows the value of v_s that reproduces $\Omega h^2 = 0.12$. Here we choose $m_\chi = 100$ GeV, $m_{h'} = 300$ GeV, and $\sin\theta = 0.1$ as a reference parameter set and vary the value of m_V. For $m_V > 2m_\chi$, V can decay into χ and thus Ωh^2 is determined by the abundance of χ. Hence Ωh^2 is independent of m_V. For $m_V < 2m_\chi$, V is also a stable particle. Thus the relic abundance of V also contributes to Ωh^2, and v_s depends on the value of m_V. We use this value of v_s for all the panels in Fig. 8.

The top-right panel in Fig. 8 shows the value of the relic abundance of V and χ. We denote them as $(\Omega h^2)_V$ and $(\Omega h^2)_\chi$, respectively. We find that $(\Omega h^2)_V > (\Omega h^2)_\chi$ for $m_\chi < m_V$. The exception is found around $m_V = m_h/2 \simeq 62.5$ GeV. This is due to the Higgs resonant enhancement in the annihilation of V. In that region of the parameter space, a VV pair efficiently annihilates into SM particles by exchanging the SM Higgs boson in the s-channel, and thus χ is the dominant component of DM.

As we discussed in Sect. 3, the V–nucleon scattering process is not suppressed by the small momentum transfer. Hence the two-component scenario is testable through the direct detection experiments. The experiments give the upper bound on the spin-independent cross section $\sigma_{\rm SI}$ under the assumption that the DM is single component. To compare the two-component scenario with the experiments, we define the effective spin-independent cross section by scaling according to the fraction of the V and χ components,

$$(\sigma_{\rm SI})_{\rm eff} = \sigma_{\rm SI}^V \frac{(\Omega h^2)_V}{(\Omega h^2)_V + (\Omega h^2)_\chi} + \sigma_{\rm SI}^\chi \frac{(\Omega h^2)_\chi}{(\Omega h^2)_V + (\Omega h^2)_\chi}, \tag{65}$$

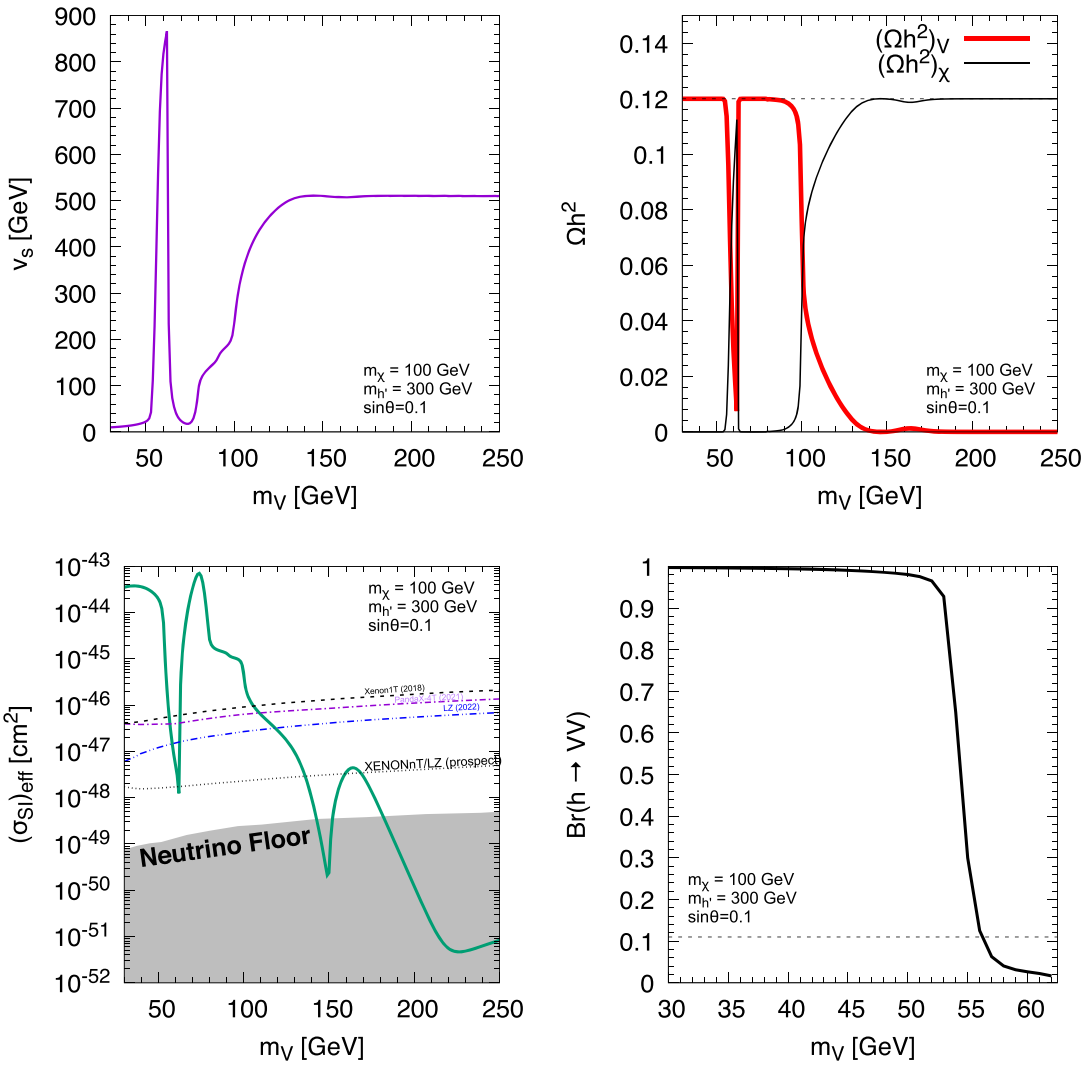

Fig. 8. Results in the two-component DM scenario. Here we choose $m_\chi = 100$ GeV, $m_{h'} = 300$ GeV, and $\sin\theta = 0.1$ as reference values. Top left: the value of v_s that reproduces the measured value of the DM energy density. Top right: the relic abundance of V and χ. Bottom left: The green solid curve shows the model prediction of $\sigma_{\rm SI}$ scaled by the fractions of the relic abundances of V and χ. Bottom right: The branching ratio of $h \to VV$. The horizontal dashed line shows the current upper bound on the branching ratio.

where $\sigma^V_{\rm SI}$ and $\sigma^\chi_{\rm SI}$ are the cross sections for $VN \to VN$ and $\chi N \to \chi N$, respectively. The latter is suppressed by the small momentum transfer but is generated at the loop level as discussed in Sect. 6. The bottom-left panel in Fig. 8 shows $(\sigma_{\rm SI})_{\rm eff}$. Compared to the recent results from the direct detection experiments [2–4], we find that the region for $m_V \lesssim 120$ GeV except for the Higgs resonant region is excluded. This is a natural consequence because V–nucleon scattering is not suppressed by the small momentum transfer. From this result and the top-right panel, we find that V cannot be the dominant component of DM in the two-component scenario in this model.

We also show Br($h \to VV$) in the bottom-right panel in Fig. 8. The partial width of $h \to VV$ is given by

$$\Gamma(h \to VV) = \frac{1}{32\pi m_h} g_{hVV}^2 \left(2 + \frac{\left(m_h^2 - 2m_V^2\right)^2}{4m_V^4}\right) \sqrt{1 - \frac{4m_V^2}{m_h^2}}. \tag{66}$$

This can be measured in the collider experiments as the Higgs invisible decay. We find that $m_V \lesssim 56$ GeV is excluded.

8. Summary

We have proposed a new pNG DM model that can explain the null results of the direct detection experiments. There is an $SU(2)_g$ global symmetry and a $U(1)_X$ gauge symmetry in the dark sector. We assume that the VEV of a complex scalar field ϕ breaks these symmetries into $U(1)_D$ global symmetry spontaneously. We also assume that the $SU(2)_g$ global symmetry is explicitly and softly broken into $U(1)_g$. Under the setup, we obtain a complex pNG scalar (χ) that is stable thanks to the $U(1)_D$ global symmetry. This χ is a DM candidate in this model. We also impose that the dark sector has a discrete symmetry defined in Eqs. (5) and (6), which can be identified as the charge conjugation in the dark sector. This discrete symmetry forbids the gauge kinetic mixing between the $U(1)_X$ in the dark sector and the $U(1)_Y$ in the visible sector. The $U(1)_X$ gauge boson can be stable thanks to this discrete symmetry if its mass is less than twice the pNG DM mass.

The advantage of our model is that the soft symmetry-breaking terms other than $\phi^\dagger \tau^3 \phi$ are forbidden by the $U(1)_X$ gauge symmetry. This restriction on the soft symmetry-breaking term guarantees suppression in the scattering amplitudes by the momentum transfer.

We have calculated the relic abundance and determined the DM coupling to the Higgs boson that reproduces the measured value of the DM energy density. Some region of the parameter space requires relatively large coupling, and thus we have also checked the perturbative unitarity bound. We have found that most of the parameter space is consistent with the PU bound. It is also found that the $U(1)_X$ gauge coupling can be large and the heavy pNG DM region is excluded by the PU bound if we assume that the mass of the gauge boson is larger than twice the mass of the pNG DM. In addition, we have considered the cosmic string in our model, which is a softly broken version of the semilocal string and is topologically stable due to the non-trivial topology of the vacuum. We have checked that the DM contribution from the cosmic string loops is insignificant. Moreover, we have discussed the loop effect on the spin-independent cross section. We have found that the effect is small unless the $U(1)_X$ gauge coupling is large.

The dark sector contains the gauge boson as well as the pNG DM. If the mass of the gauge boson is smaller than twice the pNG DM mass, then the gauge boson is also stable due to the discrete symmetry (charge conjugation) in the dark sector. Therefore the model contains the two-component DM scenario depending on the mass spectra. We briefly discussed the two-component DM scenario in Sect. 7. We showed that the results in the direct detection experiments give a strong bound on the scenario because V is not pNG DM and thus the V–nucleon scattering is not suppressed by the small momentum transfer.

The model contains the $U(1)_X$ gauge symmetry, which is not asymptotic free and would hit the Landau pole at high energy. We need a small gauge coupling or some UV completion. One possible extension of the current model is to embed the $U(1)_X$ gauge symmetry into an $SU(2)$

gauge symmetry that is broken into the $U(1)_X$ gauge symmetry spontaneously. Discussion of the possible UV picture will be discussed in the future.

Acknowledgements
The authors thank Christian Gross for a valuable comment. Y.H. would like to thank Yoshihiko Abe for useful discussions. This work is supported in part by JSPS KAKENHI Grant Numbers 19H04615 and 21K03549 (T.A.) and JP21J01117 (Y.H.). The work is also supported by the JSPS Core-to-Core Program (grant number: JPJSCCA20200002).

Funding
Open Access funding: SCOAP[3].

Appendix A. Cosmic string solution

We here discuss the solution of the cosmic string in our model. For simplicity, we concentrate on the dark sector consisting of ϕ and V_μ and ignore their portal coupling with the SM sector, $\lambda_{H\phi} = 0$. This would not change the following argument much. The effect of such a portal coupling is studied in Ref. [49].

Firstly, we rewrite the Lagrangian of the dark sector in Eq. (7) as

$$\mathcal{L}_{\rm dark} = |D_\mu \phi|^2 - \frac{1}{4} V^{\mu\nu} V_{\mu\nu} - \lambda_\phi \left(|\phi|^2 - \frac{v_s^2}{2} \right)^2 - m_\chi^2 \phi_1^2 \tag{A1}$$

with $\phi = (\phi_1, \phi_2)^t$. To discuss the string solutions, it is convenient to rescale the fields as

$$V_\mu \to \frac{2}{g_D} V_\mu, \quad \phi \to \frac{2}{g_D} \phi, \tag{A2}$$

leading to

$$\mathcal{L}_{\rm dark} = \frac{4}{g_D^2} \left[|\hat{D}_\mu \phi|^2 - \frac{1}{4} V^{\mu\nu} V_{\mu\nu} - \frac{\beta}{2} \left(|\phi|^2 - \frac{g_D^2 v_s^2}{8} \right)^2 - m_\chi^2 \phi_1^2 \right] \tag{A3}$$

with $\hat{D}_\mu = \partial_\mu + i V_\mu$. We have introduced a parameter $\beta \equiv 8\lambda_\phi / g_D^2$, which is equal to the squared mass ratio of the gauge and scalar bosons, $\beta = m_{h'}^2 / m_{V'}^2$. In the following, we take the dimensionless unit such that $g_D v_s / 2 = 1$, which is equivalent to introducing the dimensionless variables (denoted by tilde)

$$V_\mu = \frac{g_D v_s}{2} \tilde{V}_\mu, \quad x^\mu = \tilde{x}^\mu \frac{2}{g_D v_s}, \quad \phi = \frac{g_D v_s}{2} \tilde{\phi}, \quad m_\chi = \frac{g_D v_s}{2} \tilde{m}_\chi, \tag{A4}$$

for which the Lagrangian is given by

$$\mathcal{L}_{\rm dark} = g_D^2 v_s^4 \left[|\tilde{D}_\mu \tilde{\phi}|^2 - \frac{1}{4} \tilde{V}^{\mu\nu} \tilde{V}_{\mu\nu} - \frac{\beta}{2} \left(|\tilde{\phi}|^2 - \frac{1}{2} \right)^2 - \tilde{m}_\chi^2 \tilde{\phi}_1^2 \right] \tag{A5}$$

with $\tilde{D}_\mu = \tilde{\partial}_\mu + i \tilde{V}_\mu$. In the following, we drop the tildes for simplicity.

We consider the axially symmetric ansatz for the string solution,

$$\phi = \frac{1}{\sqrt{2}} \begin{pmatrix} h(r) \\ f(r) e^{i\theta} \end{pmatrix}, \quad V_\theta = -(1 - w(r)) \tag{A6}$$

and $V_r = V_z = V_t = 0$. We have introduced the cylinder coordinate $x + iy = re^{i\theta}$. The profile functions, $f(r)$, $h(r)$, and $w(r)$, should satisfy the boundary conditions

$$f(0) = 0, \qquad h'(0) = 0, \quad w(0) = 1, \tag{A7}$$

$$f(\infty) = 1, \quad h(\infty) = 0, \quad w(\infty) = 0\,. \tag{A8}$$

Since this configuration behaves asymptotically at $r \to \infty$ as

$$\phi \sim \frac{1}{\sqrt{2}} e^{i\theta} \begin{pmatrix} 0 \\ 1 \end{pmatrix}, \quad V_\theta \sim -1, \tag{A9}$$

it has the unit winding number in the vacuum manifold $U(1)_g \times U(1)_X/U(1)_D$, and hence describes a topologically stable solution. The profile functions are determined by solving the classical equations of motion (EOMs).

Before solving the EOMs, let us consider the so-called semilocal model [33,34], which is equivalent to our model with the soft symmetry-breaking term chopped off, $m_\chi \to 0$. There, the symmetry-breaking pattern is $SU(2)_g \times U(1)_X \to U(1)_D$, and the existence of the stable string solution (called the semilocal string) depends on the parameter β [50,51]. This is because of the trivial first homotopy group, $\pi_1(SU(2)_g \times U(1)_X/U(1)_D) \simeq 0$. For $\beta \leq 1$, the string is classically stable (i.e., local minimum of the energy) and is nothing but the embedding of the Abrikosov–Nielsen–Olesen (ANO) string [52,53] into ϕ_2 and V_μ with ϕ_1 vanishing everywhere. On the other hand, for $\beta > 1$, it is unstable because a condensation of ϕ_1 happens inside the core of the string and the condensed region expands outward infinitely, resulting in no static stable configuration. Thus the critical value of β for the stability is equal to the value that is the boundary for whether the condensation of ϕ_1 occurs or not (we denote it by β_b and $\beta_b = 1$ in this case).

Let us move on to our model, $m_\chi \neq 0$. In this case, m_χ gives a positive constant mass for ϕ_1 and the condensation of ϕ_1 must be suppressed. Thus the boundary value of β for the condensation, β_b, must be shifted to be larger than unity $\beta_b > 1$ depending on m_χ. Furthermore, even when the condensation occurs for $\beta > \beta_b$, it does not expand infinitely but stops at finite size $\sim m_\chi^{-1}$ because ϕ_1 must be zero at large distances from the string core due to the positive mass, as in Eq. (A9). This means that the condensation of ϕ_1 does not destabilize the string solution, which is consistent with the topological argument $\pi_1(U(1)_g \times U(1)_X/U(1)_D) \simeq \mathbb{Z}$.

Substituting the ansatz (A6), we obtain the EOMs as

$$f'' + \frac{f'}{r} - \frac{w^2}{r^2} f - \frac{\beta}{2} f\left(f^2 + h^2 - 1\right) = 0, \tag{A10}$$

$$h'' + \frac{h'}{r} - \frac{(w-1)^2}{r^2} h - m_\chi h - \frac{\beta}{2} h\left(f^2 + h^2 - 1\right) = 0, \tag{A11}$$

$$w'' - \frac{w'}{r} - (f^2 + h^2) w + h^2 = 0. \tag{A12}$$

We solve the EOMs numerically by the relaxation method and show the string solutions in Fig. A1. Note that all dimensionful quantities are normalized by $g_D v_s/2$. In the top-left panel, the condensation of $\phi_1 = h(r)/\sqrt{2}$ takes place in the string core. As β decreases or m_χ increases, the condensation is suppressed, as in the top-right and bottom panels. In the latter case, the solution is the same as the standard ANO vortex string. Figure A2 shows a parameter region in which ϕ_1 condenses inside the string core. We can see that quite a small value of m_χ suffices to suppress the condensation. Around $m_\chi \simeq 0$, the condensation can occur only for $\beta > 1$, which is consistent with the semilocal case. Note that all solutions even with the condensation are topologically stable thanks to the non-trivial winding number (A9).

The above result is similar to the one in Ref. [32] that admits semilocal strings with an explicit $SU(2)$-breaking term. There, the $SU(2)$-breaking term is given as a mass-dimension-four oper-

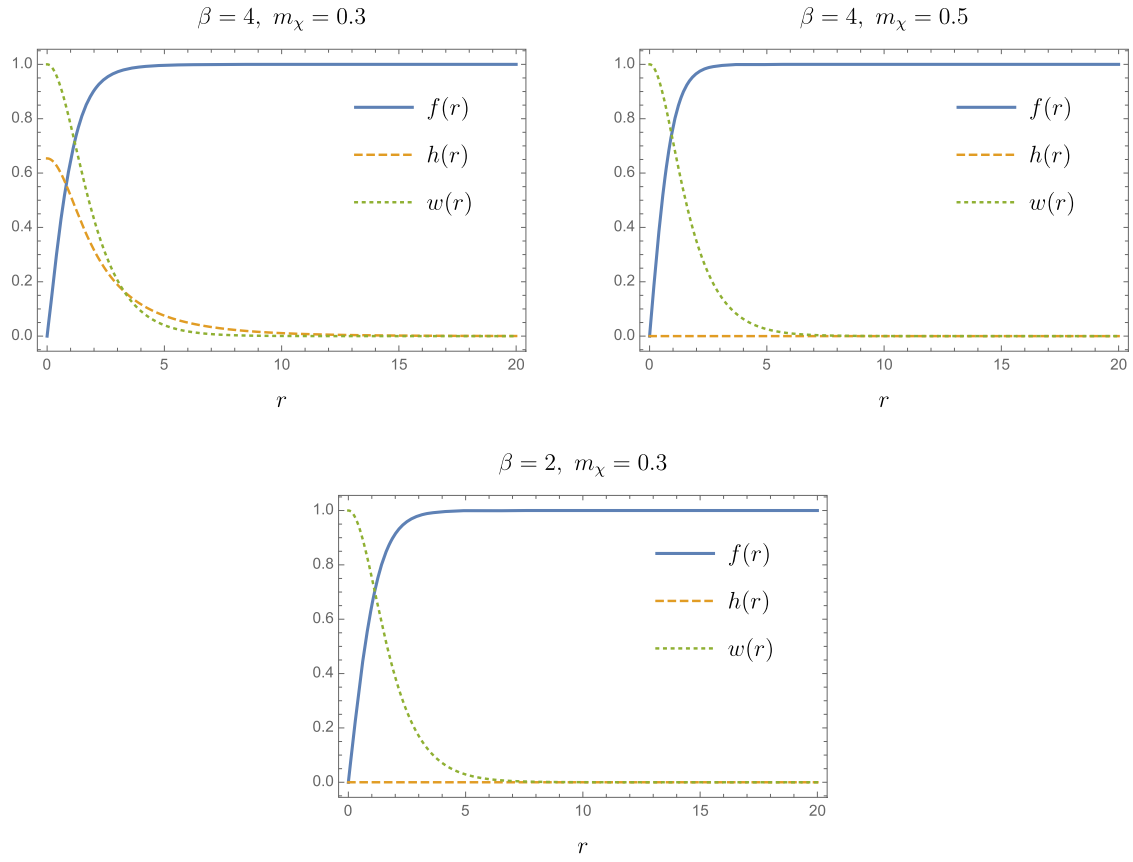

Fig. A1. Plots for the string solutions. All dimensionful quantities are normalized by $g_D v_s/2$. In the top-left panel, the condensation of $\phi_1 = h(r)/\sqrt{2}$ takes place in the string core. As β decreases or m_χ increases, the condensation is suppressed, as in the top-right and bottom panels.

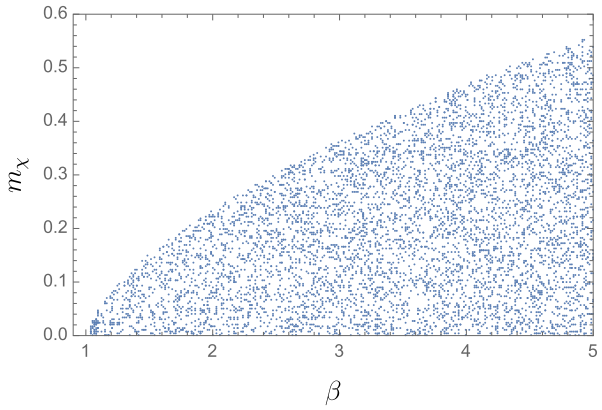

Fig. A2. Scatter plot for the parameter region $(\beta,\ m_\chi)$ in which the condensation of ϕ_1 occurs in the string core. m_χ is normalized by $g_D v_s/2$.

ator, $(\phi^\dagger T^3 \phi)^2$, and both ϕ_1 and ϕ_2 develop their VEVs at the vacuum. As a result, the solution is topologically stable and can be a "vortex molecule" consisting of two half-quantized strings depending on the parameters. On the other hand, in our model, ϕ_1 vanishes outside the string core due to the soft-breaking term $\phi^\dagger T^3 \phi$. Thus the string solution is qualitatively different from that in Ref. [32].

One may consider that the non-zero ϕ_1 in the string solution breaks the $U(1)_D$ symmetry, making it a superconducting string [54]. However, this is not the case. In the soliton background, the generator of the $U(1)_D$ symmetry should be defined as $-T^a n^a + 1/2$ with $n^a = (\phi^\dagger \tau^a \phi)/|\phi|^2$. Thus the solution given as Eq. (A6) is always invariant under this symmetry.

Appendix B. Scattering amplitudes of χ and nucleons

We here provide explicit expressions for the scattering amplitudes shown in Fig. 5. In the following, we denote $h_1 \equiv h$, $h_2 \equiv h'$. It is straightforward to calculate diagrams (a)–(d):

$$i\mathcal{M}_a = i\mathcal{M}_b = -\bar{u}u \sum_{j,k=1,2} g_{ffh_j} \frac{1}{m_{h_j}^2} g_{\chi\chi h_j h_k} g_{\chi\chi h_k} \frac{i}{(4\pi)^2} B_0\left(m_\chi^2, m_{h_k}^2, m_\chi^2\right), \tag{B1}$$

$$i\mathcal{M}_c = \bar{u}u \sum_{j=1,2} \frac{g_{ffh_j} g_{VVh_j}}{m_{h_j}^2} \frac{g_D^2}{4} \frac{i}{(4\pi)^2} \left[\left(-m_V^2 + 4m_\chi^2\right) \frac{\partial}{\partial m_V^2} B_0\left(m_\chi^2, m_V^2, m_\chi^2\right) - B_0\left(m_\chi^2, m_V^2, m_\chi^2\right) + B_0\left(0, m_V^2, m_V^2\right) \right], \tag{B2}$$

$$i\mathcal{M}_d = -\bar{u}u \sum_{j,k,l=1,2} \frac{g_{ffh_j} g_{\chi\chi h_j} g_{\chi\chi h_k} g_{h_j h_k h_l}}{m_{h_j}^2} \frac{i}{(4\pi)^2} C_0\left(m_\chi^2, m_\chi^2, 0, m_k^2, m_\chi^2, m_l^2\right), \tag{B3}$$

where u is the spinor wavefunction and

$$\frac{i}{(4\pi)^2} B_0\left(p^2, m_1^2, m_2^2\right) \equiv \int \frac{d^d l}{(2\pi)^d} \frac{1}{\left(l^2 - m_1^2\right)\left(l+p\right)^2 - m_2^2}, \tag{B4}$$

$$\frac{i}{(4\pi)^2} C_0\left(p_1^2, p_2^2, (p_1+p_2)^2, m_1^2, m_2^2, m_3^2\right) \equiv \int \frac{d^d l}{(2\pi)^d} \frac{1}{\left(l^2 - m_1^2\right)\left[(l+p_1)^2 - m_2^2\right]\left[(l+p_1+p_2)^2 - m_3^2\right]}, \tag{B5}$$

$$g_{\chi\chi hh} = 2\lambda_\phi s_\theta^2 + \lambda_{H\Phi} c_\theta^2, \tag{B6}$$

$$g_{\chi\chi hh'} = -2\lambda_\phi s_\theta c_\theta + \lambda_{H\Phi} s_\theta c_\theta, \tag{B7}$$

$$g_{\chi\chi h'h'} = 2\lambda_\phi c_\theta^2 + \lambda_{H\Phi} s_\theta^2, \tag{B8}$$

$$g_{hhh} = 6v\lambda_H c_\theta^3 - 3v_s\lambda_{H\Phi} c_\theta^2 s_\theta + 3v\lambda_{H\Phi} c_\theta s_\theta^2 - 6v_s\lambda_\Phi s_\theta^3, \tag{B9}$$

$$g_{hhh'} = 6v\lambda_H c_\theta^2 s_\theta + 6v_s\lambda_\Phi c_\theta s_\theta^2 + v_s\lambda_{H\Phi}\left(c_\theta^3 - 2c_\theta s_\theta^2\right) + v\lambda_{H\Phi}\left(s_\theta^3 - 2c_\theta^2 s_\theta\right), \tag{B10}$$

$$g_{hh'h'} = 6v\lambda_H c_\theta s_\theta^2 - 6v_s\lambda_\Phi c_\theta^2 s_\theta + v\lambda_{H\Phi}\left(c_\theta^3 - 2c_\theta s_\theta^2\right) + v_s\lambda_{H\Phi}\left(-s_\theta^3 + 2c_\theta^2 s_\theta\right), \tag{B11}$$

$$g_{h'h'h'} = 6v\lambda_H s_\theta^3 + 3v_s\lambda_{H\Phi} c_\theta s_\theta^2 + 3v\lambda_{H\Phi} c_\theta^2 s_\theta + 6v_s\lambda_\Phi c_\theta^3. \tag{B12}$$

Thus the Wilson coefficient C_q^S is obtained as

$$\begin{aligned} C_q^S = &-2\sum_{j,k=1,2}\frac{g_{ffh_j}g_{\chi\chi h_j h_k}g_{\chi\chi h_k}}{m_q m_{h_j}^2}\frac{1}{(4\pi)^2}B_0\left(m_\chi^2, m_{h_k}^2, m_\chi^2\right) \\ &+\sum_{j=1,2}\frac{g_{ffh_j}g_{VVh_j}}{m_q m_{h_j}^2}\frac{g_D^2}{4}\frac{1}{(4\pi)^2}\Bigg[\left(-m_V^2+4m_\chi^2\right)\frac{\partial}{\partial m_V^2}B_0\left(m_\chi^2, m_V^2, m_\chi^2\right) \\ &-B_0\left(m_\chi^2, m_V^2, m_\chi^2\right)+B_0\left(0, m_V^2, m_V^2\right)\Bigg] \\ &-\sum_{j,k,l=1,2}\frac{g_{ffh_j}g_{\chi\chi h_j}g_{\chi\chi h_k}g_{h_j h_k h_l}}{m_q m_{h_j}^2}\frac{1}{(4\pi)^2}C_0\left(m_\chi^2, m_\chi^2, 0, m_k^2, m_\chi^2, m_l^2\right). \end{aligned} \tag{B13}$$

On the other hand, it is relatively complicated to calculate diagram (e) with the QCD NLO contribution. It is given in Ref. [21] as

$$i\mathcal{M}_e = i\frac{\alpha_s}{\pi}G^a_{\mu\nu}G^{a\mu\nu}\sum_{j\le k}\frac{y_{tth_j}y_{tth_k}}{m_\chi^4}\frac{g_{\chi\chi h_j}g_{\chi\chi h_k}}{4}J^{jk}_{\rm box}, \tag{B14}$$

$$J^{jk}_{\rm box} \equiv \frac{(2-\delta^{jk})}{8(4\pi)^2}\int_0^\infty dt\,\frac{tI(t)}{(t+x_j)(t+x_k)}\left(1-\sqrt{\frac{t+4}{t}}\right), \tag{B15}$$

$$I(t) \equiv \frac{t-2x_t}{t(t+4x_t)}+\frac{2x_t(t+x_t)}{t^2(t+4x_t)\beta}\log\left(\frac{2x_t+t(1+\beta)}{2x_t+t(1-\beta)}\right), \tag{B16}$$

with $\beta=\sqrt{1+4x_t/t}$, $x_j\equiv m_{h_j}^2/m_\chi^2$, $x_t\equiv m_t^2/m_\chi^2$, and m_t being the top-quark mass. Compared with the result in Ref. [21], note the presence of the factor 4 in the denominator in Eq. (B14) because χ is now a complex scalar instead of a real one. Then the Wilson coefficient is obtained as

$$C_g^S = \sum_{j\le k}\frac{y_{tth_j}y_{tth_k}}{m_\chi^4}\frac{g_{\chi\chi h_j}g_{\chi\chi h_k}}{4}J^{jk}_{\rm box}. \tag{B17}$$

The loop integrations B_0 and C_0 are numerically evaluated by `LoopTools` [55].

References

[1] N. Aghanim et al., Astron. Astrophys. **641**, A6, 2020; **652**, C4 (2021) [erratum][arXiv:1807.06209] [Search inSPIRE].
[2] E. Aprile, J. Aalbers, F. Agostini, M. Alfonsi, L. Althueser, F. D. Amaro, M. Anthony, F. Arneodo, and L. Baudis, Phys. Rev. Lett. **121**, 111302 (2018) [arXiv:1805.12562] [Search inSPIRE].
[3] Y. Meng, Z. Wang, Y. Tao, A. Abdukerim, Z. Bo, W. Chen, X. Chen, Y. Chen, C. Cheng, and Y. Cheng, Phys. Rev. Lett. **127**, 261802 (2021) [arXiv:2107.13438] [Search inSPIRE].
[4] D. S. Akerib, C. W. Akerlof, A. K. Al Musalhi, F. Alder, A. Alqahtani, S. K. Alsum, C. S. Amarasinghe, A. Ames, T. J. Anderson, and N. Angelides, arXiv:2207.03764[Search inSPIRE].
[5] C. Gross, O. Lebedev, and T. Toma, Phys. Rev. Lett. **119**, 191801 (2017) [arXiv:1708.02253] [Search inSPIRE].
[6] Y. Abe and T. Toma, Phys. Lett. B **822**, 136639 (2021) [arXiv:2108.10647] [Search inSPIRE].
[7] Y. B. Zeldovich, I. Yu. Kobzarev, and L. B. Okun, Zh. Eksp. Teor. Fiz. **67**, 3 (1974).
[8] Y. Abe, T. Toma, and K. Tsumura, J. High Energy Phys. **2005**, 057 (2020) [arXiv:2001.03954] [Search inSPIRE].
[9] N. Okada, D. Raut, and Q. Shafi, Phys. Rev. D **103**, 055024 (2021) [arXiv:2001.05910] [Search inSPIRE].
[10] Y. Abe, T. Toma, K. Tsumura, and N. Yamatsu, Phys. Rev. D **104**, 035011 (2021) [arXiv:2104.13523] [Search inSPIRE].
[11] N. Okada, D. Raut, Q. Shafi, and A. Thapa, Phys. Rev. D **104**, 095002 (2021) [arXiv:2105.03419] [Search inSPIRE].

[12] A. Vilenkin and E. P. S. Shellard, Cosmic Strings and Other Topological Defects (Cambridge University Press, Cambridge, UK, 2000).
[13] A. E. Everett and A. Vilenkin, Nucl. Phys. B **207**, 43 (1982).
[14] T. W. B. Kibble, G. Lazarides, and Q. Shafi, Phys. Rev. D **26**, 435 (1982).
[15] S. Abe, G.-C. Cho, and K. Mawatari, Phys. Rev. D **104**, 035023 (2021) [arXiv:2101.04887] [Search inSPIRE].
[16] T. Alanne, N. Benincasa, M. Heikinheimo, K. Kannike, V. Keus, N. Koivunen, and K. Tuominen, J. High Energy Phys. **2010**, 080 (2020) [arXiv:2008.09605] [Search inSPIRE].
[17] L. Coito, C. Faubel, J. Herrero-Garcia, and A. Santamaria, J. High Energy Phys. **2111**, 202 (2021) [arXiv:2106.05289] [Search inSPIRE].
[18] D. Karamitros, Phys. Rev. D **99**, 095036 (2019) [arXiv:1901.09751] [Search inSPIRE].
[19] C. Cai, Y.-P. Zeng, and H.-H. Zhang, J. High Energy Phys. **2201**, 117 (2022) [arXiv:2109.11499] [Search inSPIRE].
[20] P. A. Zyla et al., Prog. Theor. Exp. Phys. **2020**, 083C01 (2020)
[21] K. Ishiwata and T. Toma, J. High Energy Phys. **1812**, 089 (2018) [arXiv:1810.08139] [Search inSPIRE].
[22] D. Azevedo, M. Duch, B. Grzadkowski, D. Huang, M. Iglicki, and R. Santos, J. High Energy Phys. **1901**, 138 (2019) [arXiv:1810.06105] [Search inSPIRE].
[23] S. Glaus, M. Mühlleitner, J. Müller, S. Patel, T. Römer, and R. Santos, J. High Energy Phys. **2012**, 034 (2020) [arXiv:2008.12985] [Search inSPIRE].
[24] B. W. Lee, C. Quigg, and H. B. Thacker, Phys. Rev. D **16**, 1519 (1977).
[25] J. M. Cornwall, D. N. Levin, and G. Tiktopoulos, Phys. Rev. D **10**, 1145 (1974); **11**, 972 (1975) [erratum].
[26] M. S. Chanowitz and M. K. Gaillard, Nucl. Phys. B **261**, 379 (1985).
[27] G. J. Gounaris, R. Kogerler, and H. Neufeld, Phys. Rev. D **34**, 3257 (1986).
[28] H. G. J. Veltman, Phys. Rev. D **41**, 2294 (1990).
[29] ATLAS Collaboration, ATLAS-CONF-2020-052, https://cds.cern.ch/record/2743055.
[30] A. Tumasyan et al., Phys. Rev. D **105,** 092007 (2022)[arXiv:2201.11585 [hep-ex]] [Search inSPIRE].
[31] J. de Blas et al., J. High Energy Phys. **2001**, 139 (2020) [arXiv:1905.03764] [Search inSPIRE].
[32] M. Eto, M. Nitta, and K. Sakurai, J. High Energy Phys. **1610**, 048 (2016) [arXiv:1608.03516] [Search inSPIRE].
[33] T. Vachaspati and A. Achucarro, Phys. Rev. D **44**, 3067 (1991).
[34] A. Achucarro and T. Vachaspati, Phys. Rept. **327**, 347 (2000) [arXiv:hep-ph/9904229] [Search inSPIRE].
[35] T. W. B. Kibble, J. Phys. A **9**, 1387 (1976).
[36] W. H. Zurek, Nature **317**, 505 (1985).
[37] A. Vilenkin and T. Vachaspati, Phys. Rev. D **35**, 1138 (1987).
[38] R. A. Battye and E. P. S. Shellard, Nucl. Phys. B **423**, 260 (1994) [arXiv:astro-ph/9311017] [Search inSPIRE].
[39] C. J. A. P. Martins and E. P. S. Shellard, Phys. Rev. D **54**, 2535 (1996) [arXiv: hep-ph/9602271] [Search inSPIRE].
[40] C. J. A. P. Martins and E. P. S. Shellard, Phys. Rev. D **65**, 043514 (2002) [arXiv:hep-ph/0003298] [Search inSPIRE].
[41] G. Bélanger, F. Boudjema, A. Goudelis, A. Pukhov, and B. Zaldivar, Comput. Phys. Commun. **231**, 173 (2018) [arXiv:1801.03509] [Search inSPIRE].
[42] T. Binder, T. Bringmann, M. Gustafsson, and A. Hryczuk, Phys. Rev. D **96**, 115010 (2017); **101**, 099901 (2020) [erratum][arXiv:1706.07433] [Search inSPIRE].
[43] T. Abe, Phys. Rev. D **104**, 035025 (2021) [arXiv:2106.01956] [Search inSPIRE].
[44] A. Hryczuk and M. Laletin, Phys. Rev. D **106**, 2 (2022) arXiv:2204.07078[Search inSPIRE].
[45] K. Ala-Mattinen and K. Kainulainen, J. Cosmol. Astropart. Phys. **2009**, 040 (2020) [arXiv:1912.02870] [Search inSPIRE].
[46] K. Ala-Mattinen, M. Heikinheimo, K. Kainulainen, and K. Tuominen,Phys. Rev. D **105**, 12 (2022) arXiv:2201.06456[Search inSPIRE].
[47] P. Gondolo and G. Gelmini, Nucl. Phys. B **360**, 145 (1991).
[48] J. Hisano, K. Ishiwata, and N. Nagata, J. High Energy Phys. **1506**, 097 (2015) [arXiv:1504.00915] [Search inSPIRE].

[49] J. M. Hyde, A. J. Long, and T. Vachaspati, Phys. Rev. D **89**, 065031 (2014) [arXiv:1312.4573] [Search inSPIRE].
[50] M. Hindmarsh, Phys. Rev. Lett. **68**, 1263 (1992).
[51] A. Achucarro, K. Kuijken, L. Perivolaropoulos, and T. Vachaspati, Nucl. Phys. B **388**, 435 (1992).
[52] A. A. Abrikosov, Sov. Phys. JETP **5**, 1174 (1957).
[53] H. B. Nielsen and P. Olesen, Nucl. Phys. B **61**, 45 (1973).
[54] E. Witten, Nucl. Phys. B **249**, 557 (1985).
[55] T. Hahn and M. Perez-Victoria, Comput. Phys. Commun. **118**, 153 (1999) [arXiv:hep-ph/9807565] [Search inSPIRE].